

RSC Advances



This is an *Accepted Manuscript*, which has been through the Royal Society of Chemistry peer review process and has been accepted for publication.

Accepted Manuscripts are published online shortly after acceptance, before technical editing, formatting and proof reading. Using this free service, authors can make their results available to the community, in citable form, before we publish the edited article. This *Accepted Manuscript* will be replaced by the edited, formatted and paginated article as soon as this is available.

You can find more information about *Accepted Manuscripts* in the [Information for Authors](#).

Please note that technical editing may introduce minor changes to the text and/or graphics, which may alter content. The journal's standard [Terms & Conditions](#) and the [Ethical guidelines](#) still apply. In no event shall the Royal Society of Chemistry be held responsible for any errors or omissions in this *Accepted Manuscript* or any consequences arising from the use of any information it contains.

A High Yield, Controllable Process for Producing Tunable Near Infrared-Absorbing Gold Nanoplates

Cite this: DOI: 10.1039/x0xx00000x

K.T. James^a, M.G. O'Toole^a, D.N. Patel^a, G. Zhang^a, A.M. Gobin^{b†}, and R.S. Keynton^{a†}

Received 00th January 2012,
Accepted 00th January 2012

DOI: 10.1039/x0xx00000x

www.rsc.org/

The purpose of this study was to optimize a new synthesis technique, "DiaSynth," to produce near-infrared (nIR) absorbing gold nanoplates with prescribed localized surface plasmon resonance (LSPR) wavelengths in higher yields over conventional synthesis methods without the need for laborious purification steps. The molecular weight cut off (MWCO; 3.5, 8, 12, 15, 25 & 50 kDa) of the regenerated cellulose membranes (RCM), temperature (25, 37, 50 & 100 °C) and surface area to volume (SA/Vol) ratio (220, 340 & 470 mm²/ml) of the RCM to the gold nanoplate solution were varied during the synthesis process to determine the effect of each parameter on gold nanoplates yield, LSPR peak placement and stability. Results indicate the ability of the RCM to remove ~99% the contaminant small gold colloid (<10 nm) produced during the synthesis process; while, producing a 72% higher yield of gold nanoplates compared to a conventional one-step fabrication process. Increasing the MWCO of the RCM from 3.5 kDa to 15 kDa was found to blue shift the LSPR peak down by 40 nm. Increasing the SA/Vol ratio and temperature blue shifted the LSPR peak wavelength by hundreds of nanometers with the nIR absorbing gold nanoplates LSPR peak occurring within the range of 650-1100 nm. It was also discovered that the gold nanoplates fabricated via the DiaSynth process with dialysis (Process 1) displayed an increase in stability over time without the need of a capping agent. With the increased gold nanoplates stability, further purification and isolation of gold nanoplates was possible through sedimentation over time. This study demonstrated that increasing the temperature, SA/Vol, and MWCO of the RCM allows production of gold nanoplates of increased purity compared to other methods and the ability to tailor the tunability of the LSPR peak to a desired wavelength.

Introduction

Over the past decade, gold nanoparticles (GNPs) have gained great interest by biomedical researchers due to their unique physical and optical properties. Due to their versatile properties, including biocompatibility, ease of functionalization, stability under atmospheric conditions and photothermal abilities, GNPs hold promising potential in biomedicine for drug delivery, photonic-based diagnostics, and theranostic applications¹⁻⁶. For drug delivery applications, GNPs have been used to improve drug solubility, stability, and biodistribution⁷⁻¹⁷. The luminescence, localized surface plasmon resonance (LSPR), surface enhanced Raman scattering (SERS) and nonlinear optical properties of metal nanoparticles make them a robust tool for diagnostic photonics applications¹⁸⁻²⁰. Specifically, GNPs have been found to enhance the sensitivity and selectivity in the detection of low concentration biomarkers, especially in lab on a chip (LOC)-based point of

care systems^{4, 21} such as detection of cancer²²⁻²⁴, viruses^{25, 26}, bacteria²⁷⁻²⁹ as well as for blood immunoassays^{30, 31}.

Due to their adaptable optical properties, GNPs have been implemented to enhance the imaging of cells^{7, 32-43} in addition to contrast agents for *in vivo* imaging applications⁴⁴⁻⁵². As a result of their unique plasmon resonance properties, GNPs have also been utilized in photothermal therapy applications for the destruction of bacteria⁵³, cells⁵⁴⁻⁶⁰ and tissue^{1, 3, 5, 61-69}. The large surface area to volume (SA/Vol) ratio and closeness in size to biomolecules allow for specifically tailored interactions at the molecular level⁷⁰.

Near infrared-absorbing gold nanoplates can be synthesized at room temperature by reacting sodium sulfide (Na₂S) or sodium thiosulfate (Na₂S₂O₃) with a gold salt, i.e. tetrachloroauric acid (HAuCl₄), in a one or two-step process^{18, 71-76}. The advantage of using sulfide compounds over conventional reducing agents is that they can form nIR-gold nanoplates without the assistance of additional templates,

capping agents, or seeds, while maintaining a strong LSPR absorption peak in the nIR range⁷⁷. The one-step synthesis method for synthesizing nIR-gold nanoplates involves the mixing of the sodium sulfide or sodium thiosulfate reagents with the gold salt for 60-90 minutes, whereas the two-step process consists of initially mixing the gold and sulfur compounds together, followed by a precisely timed second addition of sulfur compounds^{72, 75}. Both methods produce a heterogeneous mixture of GNPs containing gold spheroids, triangular plates, and rods. An overabundance of small colloidal GNPs (<10nm) are also created in the synthesis process, which can compete with nIR-gold nanoplates for binding sites on the target molecule, reduce the total amount of therapeutic particles available (for surface conjugation), and increased endothelial uptake of non-therapeutic particles can lead to greater immune response. These particles (<10nm) are therefore viewed as contaminants and need to be removed. Traditionally, small colloids are removed from the sample via multiple centrifugation steps, which is less efficient and time consuming. As a result, current GNP manufacturing techniques produce non-purified, small volumes of random wavelengths with elevated concentrations of small colloids. Given the increasing demand for these nIR-GNPs, it is necessary to create a synthesis process that generates a high yield at a prescribed LSPR with a low to non-existent amount of colloidal contaminant.

Recently, Patel⁷⁸ has demonstrated a new synthesis process, known as "DiaSynth", which employs a regenerated cellulose membrane (RCM) as a reaction vessel to increase the yield and quality ratio (optical density ratio of nIR to colloidal GNP) of the nIR-gold nanoplates. The single-step DiaSynth process was shown to increase the optical density (OD*ml) yield by 14.3 times and be equally effective, if not better, at removing colloidal gold (<10 nm) compared to conventional multi-step nanoparticle manufacturing techniques. Thus, removing the need for additional purification steps and increasing the yield of nIR-gold nanoplates. In addition, Patel's results indicated that the molecular weight cut-off (MWCO) of the RCM may influence the nIR absorbance of the nIR-gold nanoplates; however, the aforementioned study only characterized the effect of the DiaSynth process for a limited range of MWCOs (2-12 kDa). Therefore, the purpose of this work is to optimize the DiaSynth process by investigating the direct effect of the MWCO of the RCM, temperature, and SA/Vol ratio on particle size morphology, nIR LSPR peak position (tunability), particle stability, and yield.

Experimental

Chemical Supplies. The gold salt used for all experiments was hydrogen tetrachloroaurate (III) trihydrate 99.99% (HAuCl₄*3H₂O) purchased from Alfa Aesar. A 1.72 mM HAuCl₄*3H₂O solution was prepared with DI water and protected from light with aluminum foil. The sulfur reactant used in all experiments was 3 mM solution of sodium

thiosulfate pentahydrate (Na₂S₂O₃*5H₂O) purchased from Sigma-Aldrich. In all of the experiments described below, a 32.6 ml volume of the 1.72 mM gold salt solution was combined with 7.4 ml of the Na₂S₂O₃*5H₂O solution to perform the reactions for synthesizing the nIR-gold nanoplates.

Regenerated cellulose membranes. The RCMs were purchased in a tubular form with MWCO of 3.5 (Flat width (FW) 45 mm; Spectra/Por 3), 8 kDa (FW 50 mm; Spectra/Por 7), 15 kDa (FW 45 mm; Spectra/Por 7), 25 kDa (FW 34 mm; Spectra/Por 7), and 50 kDa (FW 34 mm; Spectra/Por 7) from Spectrum Labs. A 12kDa MWCO RCM (FW 43 mm) from Sigma-Aldrich was also employed since, in our previous study, it demonstrated the ability to provide a high quality ratio (QR= Abs^{nIR}/Abs⁵³⁰) of nIR-gold nanoplates to colloidal gold⁷⁸. The RCM dialysis tubing was stored at 4°C and pretreated by soaking in 2 L of DI water for 4 days, while changing the DI water every day to remove the preservatives (glycerol, sodium azide, and/or sulfur in trace amounts). Once hydrated, the membrane was stored in a sealed plastic bag at 4°C filled with 2 L of DI water. Before use, the membrane was cut to the desired length (100, 150, or 200 mm) and rinsed thoroughly, both inside and outside, under running DI water for 30 seconds.

Conventional One-Step nIR-Gold Nanoplates Synthesis. A conventional one-step nIR-gold nanoplates synthesis process was employed as previously described⁷⁸. In brief, the volumes and concentrations of the gold salt and sodium thiosulfate solutions reported above were placed in a 200 ml glass beaker and mixed with the magnetic stir bar for 1 hr at room temperature. Upon completion of the reaction, the nIR-gold nanoplates solution was stored in 50 ml test tubes at room temperature. Samples of the nIR-gold nanoplates solution were drawn from the test tubes, then imaged and analyzed according to the procedures outlined in the Instrumentation and Imaging section below.

DiaSynth Process. After the RCMs were cut to the desired lengths, one end of the membrane was closed with a weighted dialysis clip and filled with the gold salt solution. The Na₂S₂O₃ solution was then added into the membrane via pipette followed by mixing of the solution within the RCM by manually stirring with the tip of the pipette and aspirating with the pipette pump. Subsequently, air was removed from the tubing and the other end of the membrane was clipped. To determine the effects of temperature and SA/Vol ratio of the RCM to the nIR-gold nanoplate solution, only the 12 kDa MWCO RCM was employed since it demonstrated the ability to provide a high quality ratio (QR= Abs^{nIR}/Abs⁵³⁰) of nIR-gold nanoplates to colloidal gold⁷⁸. The 12 kDa RCM tubing has a flat width of 43 mm, and by varying the length (100, 150, and 200 mm) of RCM used for the DiaSynth process, SA/Vol ratios of 220, 340, and 470 mm²/ml were obtained. For the DiaSynth

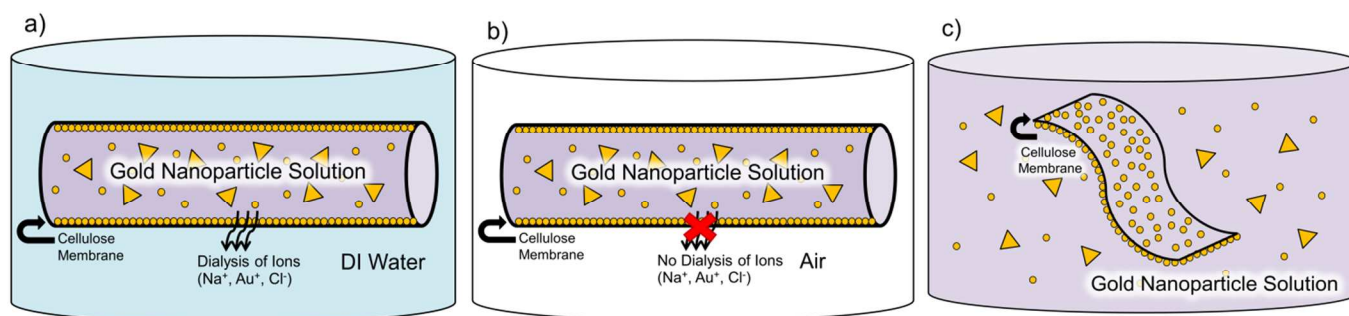


Fig. 1 nIR-gold nanoplates are synthesized in a RCM tubing with both ends clipped inside of a glass beaker, (a) Process 1 is dialyzed against water and (b) Process 2 is dialyzed against air. Process 3 (c) synthesizes nIR-gold nanoplates with the conventional one-step method inside a beaker with a RCM present within the reaction solution.

experiments with dialysis (Process 1), the filled, sealed membrane was placed in an 8 L beaker filled with 7 L of DI water with a stir bar at the bottom of the beaker rotating at 200 RPM and allowed to react for 1 hour as shown in Fig. 1a. Process 1 experiments were conducted at four different temperatures (25, 37, and 50°C) to investigate the effect of fabricating the nIR-gold nanoplates at room temperature, body temperature, and at elevated temperatures since preliminary tests yielded nIR-gold nanoplates with a wide nIR absorption range at these temperatures. For the DiaSynth without dialysis (Process 2) experiments shown in Fig. 1b, the filled, sealed RCM was placed inside a glass beaker without DI water in an oven set to 25, 50, or 100 °C. After the DiaSynth process with or without dialysis was completed, the nIR-gold nanoplate solution was stored in 50 ml test tubes (VWR International, Atlanta, GA) at room temperature. Samples of the nIR-gold nanoplate solution were drawn from the test tubes, then imaged and analyzed according to the procedures outlined in the Instrumentation and Imaging section below.

Instrumentation and Imaging. UV absorption spectra were measured on 1 ml samples at a 10x dilution in DI water with the UV Visible Spectrometer (Varian Cary 50 BIO UV, McKinley Scientific, Sparta, NJ). The size and zeta potential measurements were acquired on 1 ml samples at a 10x dilution in DI water on a zetasizer (Zetasizer Nano ZS90, Malvern Instruments Ltd., Westborough, MA). Scanning electron microscopy (SEM) was performed at 150k magnification on the Zeiss SUPRA FE-SEM (Peabody, MA) at 15 kV to determine GNP morphology and distribution. Sample preparation for the STEM measurements consisted of pipetting 50 microliters of nIR-GNP suspension onto a C-flat Holey carbon film enhanced TEM grids followed by a room temperature drying overnight. The dried samples were imaged in the STEM. Subsequently, the images were imported into ImageJ software⁷⁹ to determine size distribution and nIR-gold nanoplate yield in a 5 micron square region manually selected by the operator. Statistical analysis was performed with Minitab software⁸⁰.

Results and Discussion

Effect of Surface Area to Volume Ratio on nIR-Gold Nanoplate Tunability. Figure 2 shows the nIR peak after the synthesis of nIR-gold nanoplates via the conventional one-step process in the presence of the RCM (Process 3) with SA/Vol ratios of 0, 220, 340, 470, 650, and 1075 mm²/ml. The SA/Vol ratio of zero refers to the control sample with no RCM present. Performing an analysis of variance (ANOVA) on this data shows that increasing the SA/Vol ratio causes a significant ($P < 0.001$; $R^2 = 99.89\%$) blue shift of the nIR peak from 1100 to 800 nm. Similarly, increasing SA/Vol ratio for the DiaSynth process, both with and without dialysis, results in a blue shift of the nIR peak with the ANOVA yielding R-square values of 98.03% and 97.53%, respectively, at a significance of $p < 0.001$ for both processes (Figs. 3a and 3b). This shift is most likely due to the increased surface area allowing for additional reaction and/or seeding sites for the GNPs. Previous studies have shown that the RCM selectively adsorbs small gold colloid rather than larger nIR-gold nanoplate particles⁷⁸. Additionally, it has been reported that the carbonyl and hydroxyl groups on the cellulose polymer membrane are able to first bind to and trap gold ions, and subsequently reduce them *in situ* to begin seed formation⁸¹. The creation of a larger number of seed particles will, in turn, limit the amount of gold

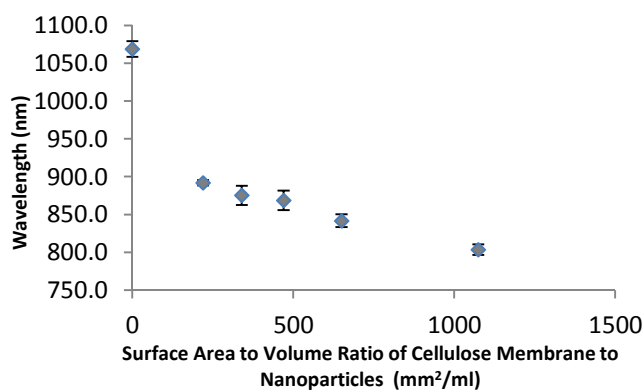


Fig. 2 nIR LSPR peak of nIR-gold nanoplates synthesized with a conventional one-step synthesis method in 50 mL test membrane in the presence of RCM. Varying SA/Vol ratios of cellulose membrane to GNP solution were used: 0, 220, 340, 470, 650, and 1075 mm²/mL. (n=3). (Note: The corresponding UV/Vis spectra for the data presented in Fig. 2 can be found in Fig. S2.)

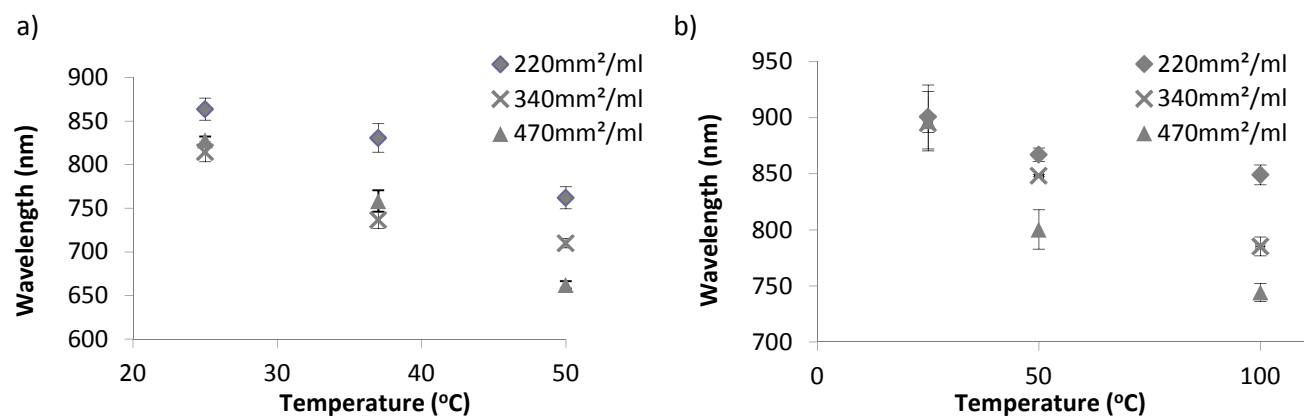


Fig. 3 Temperature vs. nIR-gold nanoplate LSPR peak placement for 220, 340, and 470 mm²/mL DiaSynth with (a) dialysis (Process 1) in 7 L of DI water and (b) without dialysis (Process 2). (n=3) (Note: The corresponding UV/Vis spectra for the data presented in Figs. 3a & 3b can be found in Figs. S3 & S4.)

available for particle growth in solution, which will directly affect the feature sizes of the nIR-gold nanoplates. Moreover, it has been shown previously that feature size is crucial for determining the position of the nIR LSPR peak, particularly for nIR-gold nanoplates, with smaller feature sizes leading to a blue shift^{82, 83}.

Effect of Temperature on the DiaSynth Process and nIR-Gold Nanoplate Tunability. The temperature effects on the nIR LSPR peak placement for nIR-gold nanoplates synthesized via the DiaSynth process with dialysis (Process 1) are shown in Fig. 3a. Temperatures above 50 °C for Process 1 lead to immediate aggregation. The data shows an increase in temperature yields a blue shift in the nIR peak from 875 to 650 nm. This is likely due to the increased reaction rate from the increase in reaction temperature leading to a higher number of seed formation events occurring on the membrane, while reducing the particle growth in solution. An ANOVA was performed and showed that temperature has a significant effect on the LSPR absorption peak with a $P < 0.001$ and R^2 value of 98.03%.

To determine if the dialysis process is crucial to the success of DiaSynth (Process 1), the DiaSynth reaction was also performed with no dialysate solution (Process 2) at various temperatures (25, 50 and 100 °C) shown in Fig. 3b. The optical spectra of the samples indicate that the nIR-gold nanoplates are still formed efficiently without the presence of dialysate. The temperature range is found to tune the nIR peak anywhere from 740-950 nm. The ANOVA data shows that temperature has a significant effect on the nIR LSPR absorption peak with a $P < 0.001$ and R^2 value of 97.53%. However, results indicate a non-linear relationship between temperature and the nIR peak for the non-dialysis DiaSynth (Process 2) experiments (Fig. 3b). Although the non-linearity may also be due to the high reaction rate from the increased temperature leading to higher seed growth on the membrane, the available SA/Vol ratio is also important. For the 220 mm²/ml SA/Vol reaction, the increase in temperature from 25 to 100 °C observed no pronounced blue shift of the LSPR, possibly because the membrane may have

become saturated with gold colloid, which would lead to more gold available in solution for particle growth. For the 470 mm²/ml a pronounced blue shift of the LSPR happens from 25 to 100 °C, because the larger surface area is available to accommodate more seed formation, leading to less available gold for particle growth and therefore smaller particles. Other factors that could contribute to the non-linearity are: 1) evaporation of water out of the solution which would increase the gold salt and sodium thiosulfate concentrations, thereby increasing the reactions between molecules and hence, promote more seed formation; 2) no dialyzing of reactants and GNPs, which could result in a retention of ions in solution weakening interparticle electrostatic repulsion, and thus, particle aggregation in solution; and/or, 3) no surrounding DI water acting as a temperature buffer during the reaction. Each of these could additionally effect the LSPR position.

The absence of dialysate in Process 2 allows exploration of higher temperatures (100 °C) than does the dialyzed reaction mixture due to the differences in heating methods for the two techniques. The non-dialyzed reaction (Process 2) temperature is established in a dry oven, whereas the dialyzed reaction temperature is established via heating the dialysate (DI water) with a hotplate (Process 1). The boiling of the dialysate under

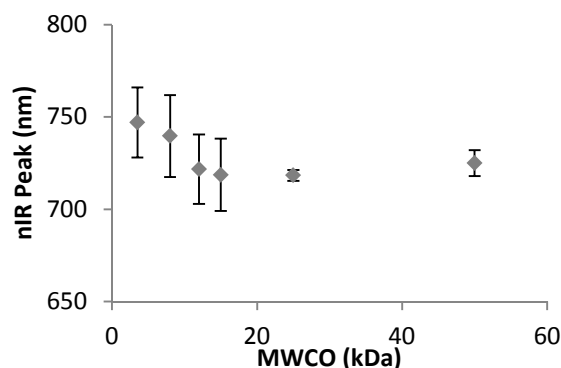


Fig. 4 MWCO vs nIR-gold nanoplate LSPR peak placement for DiaSynth with dialysis (Process 1) with 8 L of DI water (n=3). (Note: The corresponding UV/Vis spectra for the data presented in Fig. 4 can be found in Fig. S5.)

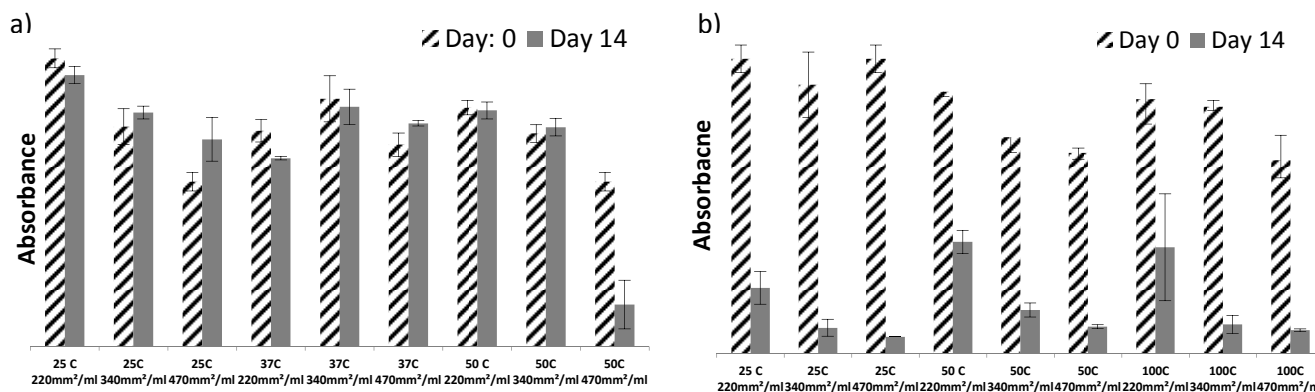


Fig 5 Stability of the GNPs with DiaSynth (a) with dialysis (Process 1) and (b) without dialysis (Process 2) measured at the nIR LSPR peak on Day 0 and 14. (n=3) (Note: The corresponding UV/Vis spectra for the data presented in Figs. 5a & 5b can be found in Figs. S6 & S7.)

these conditions adds additional convection and mixing forces that are not present for the other temperatures, which lead to a significant increase in aggregation of the nanoparticles and therefore a decrease in stability. Thus, the 100°C temperature results were omitted from the graphs of the dialysis method. On the other hand, the non-dialyzed reactions performed at 100°C yielded non-aggregated GNPs resulting in a higher stability.

Effect of MWCO on Tuning the nIR-Gold Nanoplates.

After the effects of SA/Vol and temperature on nIR LSPR peak placement were investigated, the effect of MWCO on the samples was tested. For these experiments, the MWCO of the RCM was adjusted (3.5, 8, 12, 15, 25, and 50 kDa) while the same volumes and concentrations of the HAuCl_4 and $\text{Na}_2\text{S}_2\text{O}_2$ solutions were utilized and SA/Vol and temperature were held constant at 340 mm²/ml and 40°C, respectively. Overall, the nIR LSPR peak appears to linearly decrease as the MWCO increases from 3.5 kDa to 15 kDa, then the nIR LSPR peak magnitude levels off as the MWCO increases from 15 kDa to 50 kDa (Fig. 4). However, the effect of the MWCO on the nIR LSPR peak shift is relatively small, ~40 nm; indicating that MWCO does not significantly affect the nIR LSPR peak compared to the SA/Vol ratio and temperature.

Stability of nIR-Gold Nanoplates from DiaSynth.

Immediately after completion of the reaction, the optical spectrum of the nIR-gold nanoplates was measured. Additionally, samples of nIR-gold nanoplates were placed in 50 ml test tubes and allowed to sit at room temperature for 14 days. After 14 days, optical spectra were acquired on these

samples. The samples subjected to DiaSynth with dialysis (Process 1) remained stable without being capped for 2 weeks, suggesting the gold nanoplates are stable through electrostatic repulsion with an average zeta potential of -35 mV (Fig. 5a)⁸⁴. An ANOVA concludes that there is no significant difference from Day 0 to 14 given the p-value of 0.281. The samples synthesized via the DiaSynth process without dialysis (Process 2) were unstable and aggregated within 14 days (Figure 5b). An ANOVA shows that there is a significant difference between Day 0 and 14 given the p-value ($P < 0.001$). This instability in Process 2 may be due to the lack of removal of ions from the GNP solution. The ions presence can mask the surface charge of the particles leading to reduction in interparticle repulsion and greater sample instability^{85, 86}. Thus, removal of these ions through dialysis increases bare product stability over time.

nIR-Gold Nanoplate Yield. The colloidal gold (<10 nm) contaminant in the traditional one-step synthesis process is readily apparent in STEM imaging, Fig. S1. Conversely, the DiaSynth processes both with and without dialysis (Process 1 & 2) have a lower amount of colloidal gold formation as compared to conventional one-step nIR-gold nanoplate synthesis. The yield data for the nIR-gold nanoplate synthesis is shown in Table 1. Note that the colloidal gold (<10 nm) count is not a part of the morphology (sphere, plate, or rod) percentage since the colloidal gold is a contaminant with respect to the nIR absorbing fraction. The colloidal gold count was 100x lower for the DiaSynth methods compared to conventional one-step nIR-gold nanoplate synthesis.

Table 1: The GNP colloidal gold count, particle morphology yield, and feature sizes.

Method	Colloid (<10 nm)	Sphere		Plate		Rod	
		Count	%	Diameter Size (nm)	%	Diameter or Apex (nm)	%
DiaSynth with Dialysis (Process 1)	432	68.1	32.8	28.4	47.9	3.5	70.7
DiaSynth without Dialysis (Process 2)	637	69.3	30.3	29.5	63.9	1.2	109.3
Conventional One-Step GNP Synthesis	49160	81.4	19.6	16.5	37.4	2.1	39.4

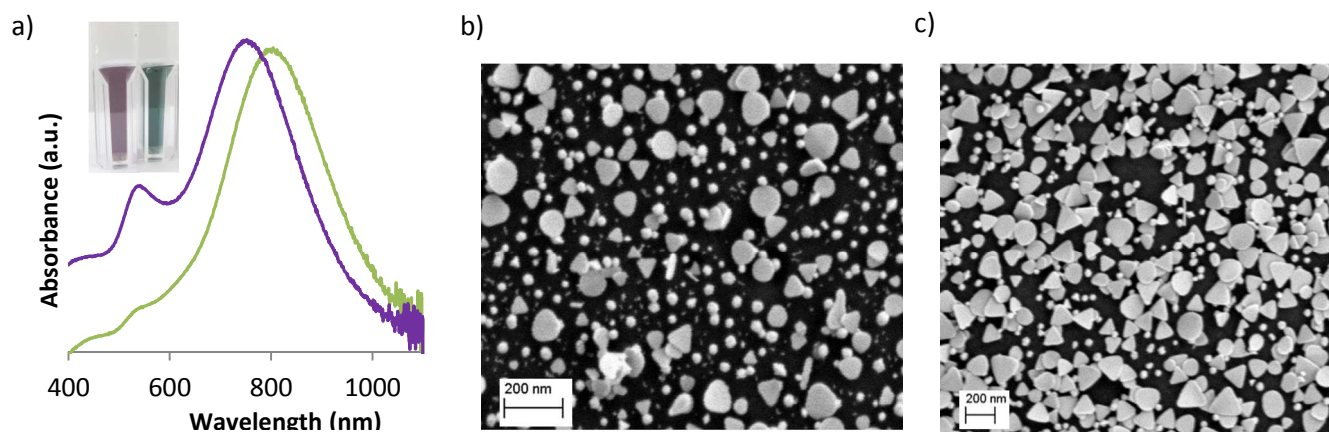


Fig. 6. (a) UV/Vis spectra of nIR-gold nanoplates before (Purple) and after (Green) sedimentation. The photograph (inset) of nIR-gold nanoplate solutions before (Left) and after (Right) sedimentation. SEM images of the gold nanoplates from (b) supernatant and (c) resuspended pellet after sedimentation.

There was no significant difference in colloidal gold count or morphology percentage between Process 1 & 2, i.e. with or without dialysis ($P > 0.05$); however, both produce significantly lower amounts of gold colloids and a higher number nIR-gold nanoplates as compared to the conventional synthesis process ($P < 0.05$). Thus, the Diasynth process was found to increase the yield of nIR-gold nanoplates by 72% compared to conventional nIR-GNP batch reaction processes using the particle counting method.

Sedimentation. In solution, the nIR-gold nanoplate sediment over time, forming a concentrated pellet. The spheroidal nanoparticles and small colloidal gold (<10nm) settle out at a much slower rate than the nIR-gold nanoplates, allowing for separation between the population subtypes without the need for centrifugation or surface coating for further purification (Fig. 6). Subsequently, the nIR absorbance peak can be tailored anywhere in the 600-1000nm range and is attributed to the nIR-gold nanoplate while the 530nm peak is attributed to the spheroidal and colloidal GNPs. Figure 7 shows the supernatant absorbance over time, with a steady decrease in nIR peak absorbance. Particle size analysis data of the suspended particles from both before and after sedimentation is detailed in Table 2. The mean size (Z-Avg.) increases in the sediment particles because the sample is going towards a monodisperse solution of nIR-gold nanoplates, by removing the other subpopulation of GNPs. Whereas, the supernatant is polydisperse with nanospheres, nanorods, and nanoplates, where

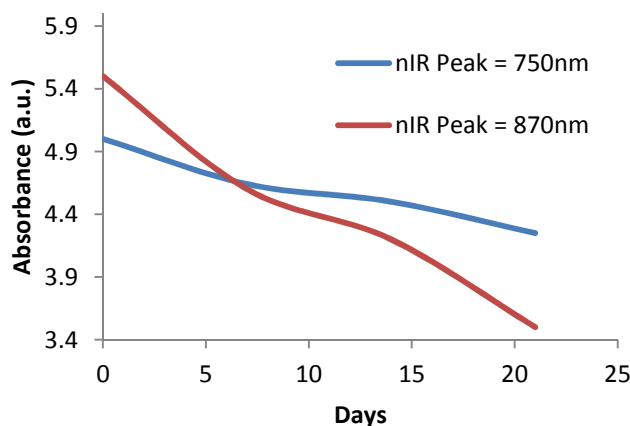


Fig. 7. Supernatant absorbance of two samples with nIR-gold nanoplates sedimenting over time. (Note: The corresponding UV/Vis spectra for the data presented in Fig. 7 can be found in Fig. S8.)

nanospheres are the largest fraction within the GNP solution. All particle samples displayed a loss in nIR intensity over time and a corresponding shift in the DLS measurements. The larger nIR-gold nanoplates settle out at a much faster rate than the smaller GNPs, most likely due to the larger geometry and mass. The Diasynth process (Process 1), in combination with sedimentation, allows for a higher yield of bare nIR-gold nanoplates. On the other hand, bare nIR-gold nanoplates produced via conventional fabrication methods aggregate, so alternative methods of separation must be employed, such as

electrophoresis⁷² or precipitation^{87, 88}, which require coating of the nIR-gold nanoplates. The sedimentation technique is a viable separation process for nIR-gold nanoplates fabricated via the DiaSynth process due to the removal of salts in the fabrication method, thereby eliminating unintended aggregation.

Table 2. Particle size analysis data of the suspended particles from both before and after sedimentation.

Sample	Sedimented nIR-gold nanoplates Pellet		Supernatant	
	nIR Peak (nm)	Z-Avg. (nm)	nIR Peak (nm)	Z-Avg. (nm)
1	801	99.4	746	89.6
2	945	121.0	862	96.9

Conclusions

The SA/Vol ratio of the RCM to nIR-gold nanoplate solution and temperature were found to significantly affect the nIR LSPR peak placement ranging from 650 to 1100nm, allowing for the production of nIR-gold nanoplates at prescribed LSPR wavelengths with high reproducibility. Although this study did not directly investigate the optimal conditions for yielding specific LSPRs, the results clearly indicate that both temperature and SA/Vol ratio are high priority since changing either parameter will have a dramatic effect on LSPR placement. Specifically, in this study, the optimal conditions for LSPR peak placement within 650-850nm consisted of using a 470mm²/ml SA/Vol ratio while varying the temperature between 25-50 °C via Process 1. However, maintaining a constant temperature and varying the SA/Vol ratio in Process 3 provided optimal conditions for achieving LSPRs above 850nm. The MWCO of the cellulose membranes did have an effect on nIR placement of nIR-gold nanoplates; however, this effect was less significant compared to SA/Vol ratio or temperature. The dialysis of ions out of the nIR-gold nanoplate solution was shown to affect the stability of non-capped gold nanoplates. The gold nanoplates produced via the DiaSynth dialysis process (Process 1) remained stable for up to 2 weeks compared to the gold nanoplates created via the non-dialysis DiaSynth process (Process 2). The DiaSynth process parameters can be carefully controlled to tailor the nIR LSPR peak to a desired value, while also increasing nIR gold nanoplate yield by 72% and reducing the colloidal gold (<10nm) by 100x. Thereby, removing the need for the additional purification steps associated with conventional processing techniques. Sedimentation of the nIR gold nanoplates were found to be sufficient for further separation of the different nanoparticle populations.

Acknowledgements

The authors would like to acknowledge Mr. Alex Keynton and Dr. Thomas Roussel for their contributions to the research.

Funding Sources

This work was funded by the grant from NSF-EPSCoR No. 0814194, NASA No. NNX10AJ36G and the Department of Bioengineering.

Notes and References

^a Department of Bioengineering, University of Louisville, Louisville, KY 40292, United States

^b Dr. Andre M. Gobin current address: TPC Group 5151 San Felipe, Suite 800 Houston, TX 77056 E-mail: Andre.Gobin@tpcgrp.com

† Drs. Gobin and Keynton are co-senior authors of this work.

Corresponding Author: Robert S. Keynton, Ph.D. 419 Lutz Hall Department of Bioengineering University of Louisville, Louisville, KY 40292 E-mail: Rob.Keynton@louisville.edu

1. A. M. Gobin, E. M. Watkins, E. Quevedo, V. L. Colvin and J. L. West, *Small*, 2010, **6**, 745-752.
2. X. Liu, M. Atwater, J. Wang and Q. Huo, *Colloids Surf B Biointerfaces*, 2007, **58**, 3-7.
3. L. R. Hirsch, R. J. Stafford, J. A. Bankson, S. R. Sershen, B. Rivera, R. E. Price, J. D. Hazle, N. J. Halas and J. L. West, *Proc Natl Acad Sci U S A*, 2003, **100**, 13549-13554.
4. F. Inci, O. Tokel, S. Wang, U. A. Gurkan, S. Tasoglu, D. R. Kuritzkes and U. Demirci, *ACS Nano*, 2013, **7**, 4733-4745.
5. A. M. Gobin, M. H. Lee, N. J. Halas, W. D. James, R. A. Drezek and J. L. West, *Nano Lett*, 2007, **7**, 1929-1934.
6. P. Ghosh, G. Han, M. De, C. K. Kim and V. M. Rotello, *Adv Drug Deliv Rev*, 2008, **60**, 1307-1315.
7. W. Cai, T. Gao, H. Hong and J. Sun, *Nanotechnol Sci Appl.*, 2008, **1**, 17-32.
8. R. Visaria, J. C. Bischof, M. Loren, B. Williams, E. Ebbini, G. Paciotti and R. Griffin, *Int J Hyperther.*, 2007, **23**, 501-511.
9. R. K. Visaria, R. J. Griffin, B. W. Williams, E. S. Ebbini, G. F. Paciotti, C. W. Song and J. C. Bischof, *Mol Cancer Ther*, 2006, **5**, 1014-1020.
10. G. F. Paciotti, L. Myer, D. Weinreich, D. Goia, N. Pavel, R. E. McLaughlin and L. Tamarkin, *Drug Deliv*, 2004, **11**, 169-183.
11. A. MS and S. N, *Pak J Pharm Sci*, 2006, **19**, 258-268.
12. R. Goel, D. Swanlund, J. Coad, G. F. Paciotti and J. C. Bischof, *Mol Cancer Ther*, 2007, **6**, 2039-2047.
13. Y.-H. Chen, C.-Y. Tsai, P.-Y. Huang, M.-Y. Chang, P.-C. Cheng, C.-H. Chou, D.-H. Chen, C.-R. Wang, A.-L. Shiau and C.-L. Wu, *Mol Pharm*, 2007, **4**, 713-722.
14. S. Sershen, S. Westcott, N. Halas and J. West, *J Biomed Mater Res*, 2000, **51**, 293-298.
15. M. Bikram, A. M. Gobin, R. E. Whitmire and J. L. West, *J Control Release*, 2007, **123**, 219-227.
16. B. Chithrani, A. Ghazani and W. Chan, *Nano Lett.*, 2006, **6**, 662-668.
17. Y. Liu, M. K. Shipton, J. Ryan, E. D. Kaufman, S. Franzen and D. L. Feldheim, *Anal Chem.*, 2007, **79**, 2221-2229.
18. R. D. Averitt, D. Sarkar and N. J. Halas, *Phys Rev Lett*, 1997, **78**, 4217-4220.
19. Y. C. Cao, R. Jin and C. A. Mirkin, *Science*, 2002, **297**, 1536-1540.
20. T. Klar, M. Perner, S. Grosse, G. von Plessen, W. Spirkl and J. Feldmann, *Phys Rev Lett*, 1998, **80**, 4249-4252.
21. E. Ozbay, *Science*, 2006, **311**, 189-193.
22. T. Kumeria, M. D. Kurkuri, K. R. Diener, L. Parkinson and D. Losic, *Biosens Bioelectron*, 2012, **35**, 167-173.
23. S. Riethdorf, H. Fritsche, V. Muller, T. Rau, C. Schindlbeck, B. Rack, W. Janni, C. Coith, K. Beck, F. Janicke, S. Jackson, T. Gornet, M. Cristofanilli and K. Pantel, *Clin Cancer Res*, 2007, **13**, 920-928.
24. X. Liu, Q. Dai, L. Austin, J. Coutts, G. Knowles, J. Zou, H. Chen and Q. Huo, *J Am Chem Soc*, 2008, **130**, 2780-2782.
25. A. M. Abraham, R. Kannangai and G. Sridharan, *Indian J Med Microbi*, 2008, **26**, 297-301.
26. A. A. Yanik, M. Huang, O. Kamohara, A. Artar, T. W. Geisbert, J. H. Connor and H. Altug, *Nano Lett*, 2010.

27. Y. C. Chang, C. Y. Yang, R. L. Sun, Y. F. Cheng, W. C. Kao and P. C. Yang, *Sci Rep*, 2013, **3**, 1863.
28. R. Maalouf, C. Fournier-Wirth, J. Coste, H. Chebib, Y. Saikali, O. Vittori, A. Errachid, J.-P. Cloarec, C. Martelet and N. Jaffrezic-Renault, *Anal Chem*, 2007, **79**, 4879-4886.
29. D. Ivnitiski, I. Abdel-Hamid, P. Atanansov and E. Wilkins, *Biosens Bioelectron*, 1999, **14**.
30. J. Chen, C. Wang and J. Irudayaraj, *J Biomed Opt*, 2009, **14**, 040501.
31. L. R. Hirsch, J. B. Jackson, A. Lee, N. J. Halas and J. L. West, *Anal Chem*, 2003, **75**.
32. G. Peleg, A. Lewis, M. Linial and L. M. Loew, *Proc Natl Acad Sci U S A*, 1996, **93**, 6700-6704.
33. L. Cagnet, C. Tardin, D. Boyer, D. Choquet, P. Tamarat and B. Lounis, *Proc Natl Acad Sci U S A*, 2003, **100**, 11350-11355.
34. P. Yang, X. Sun, J. Chiu, H. Sun and Q. He, *Bioconjug Chem*, 2005, **16**.
35. C. Loo, L. Hirsch, M. Lee, E. Chang, J. West, N. Halas and R. Drezek, *Opt Lett*, 2005, **30**.
36. A. Dunn and S. JA, *Nat Struct Mol Biol* 2007, **14**, 246-248.
37. K. Sokolov, M. Follen, J. Aaron, I. Pavlova, A. Malpica, R. Lotan and R. Richards-Kortum, *Cancer Res*, 2003, **63**, 1999-2004.
38. N. Nitin, D. J. Javier, D. M. Roblyer and R. Richards-Kortum, *J Biomed Opt*, 2007, **12**, 051505.
39. J. M. de la Fuente, C. C. Berry, M. O. Riehle and A. S. G. Curtis, *Langmuir*, 2006, **22**, 3286-3293.
40. X. Shi, S. Wang, S. Meshinchi, M. Van Antwerp, X. Bi, I. Lee and J. J. Baker, *Small*, 2007, **3**, 1245-1252.
41. N. J. Durr, T. Larson, D. K. Smith, B. A. Korgel, K. Sokolov and A. Ben-Yakar, *Nano Lett*, 2007, **7**, 941-945.
42. A. Oyelere, P. Chen, X. Huang, I. El-Sayed and M. El-Sayed, *Bioconjug Chem*, 2007, **18**, 1490-1497.
43. P. Li, C. Wei, C. Liao, C. Chen, K. Pao, C. Wang, Y. Wu and D. Shieh, *IEEE Trans Ultrason Ferroelectr Freq Control*, 2007, **54**, 1642-1647.
44. Z. Liu, W. Cai, L. He, N. Nakayama, K. Chen, K. Sun, X. Chen and H. Da, *Nat Nanotechnol*, 2007, **2**, 47-52.
45. C. Su, H. Sheu, C. Lin, C. Huang, Y. Lo, Y. Pu, J. Weng, D. Shieh, J. Chen and C. Yeh, *J Am Chem Soc*, 2007, **129**, 2139-2146.
46. X. Qian, X. H. Peng, D. O. Ansari, Q. Yin-Goen, G. Z. Chen, D. M. Shin, L. Yang, A. N. Young, M. D. Wang and S. Nie, *Nat Biotechnol*, 2008, **26**, 83-90.
47. S. Keren, C. Zavaleta, Z. Cheng, A. de la Zerda, O. Gheysens and S. S. Gambhir, *Proc Natl Acad Sci U S A*, 2008, **105**, 5844-5849.
48. P. Taroni, G. Danesini, A. Torricelli, A. Pifferi, L. Spinelli and R. Cubeddu, *J Biomed Opt*, 2004, **9**, 464-473.
49. X. Intes, *Acad Radiol*, 2005, **12**, 934-947.
50. W. Cai, K. Chen, Z. B. Li, S. S. Gambhir and X. Chen, *J Nucl Med*, 2007, **48**, 1862-1870.
51. W. Cai and C. X., *Small*, 2007, **3**, 1840-1854.
52. W. Cai and X. Chen, *J Nucl Med*, 2008, **49**, 113S-128S.
53. V. P. Zharov, K. E. Mercer, E. N. Galitovskaya and M. S. Smeltzer, *Biophys J*, 2006, **90**, 619-627.
54. L. Tong, Y. Zhao, T. B. Huff, M. N. Hansen, A. Wei and J. X. Cheng, *Adv Mater*, 2007, **19**, 3136-3141.
55. J. Chen, D. Wang, J. Xi, L. Au, A. Siekkinen, A. Warsen, Z. Li, H. Zhang, Y. Xia and X. Li, *Nano Lett*, 2007, **7**, 1318-1322.
56. X. Huang, W. Qian, I. El-Sayed and M. El-Sayed, *Lasers Surg Med*, 2007, **39**, 747-753.
57. X. Huang, P. Jain, I. El-Sayed and M. El-Sayed, *Photochem Photobiol*, 2006, **82**, 412-417.
58. X. Huang, I. El-Sayed, W. Qian and M. El-Sayed, *J Am Chem Soc*, 2006, **28**, 115-120.
59. C. Loo, A. Lowery, N. Halas, J. West and R. Drezek, *Nano Lett*, 2005, **5**, 709-711.
60. J. Stern, J. Stanfield, Y. Lotan, S. Park, J. Hsieh and J. Cadeddu, *J Endourol*, 2007, **21**, 939-943.
61. M. Camerin, S. Rello, A. Villanueva, X. Ping, M. E. Kenney, M. A. Rodgers and G. Jori, *Eur J Cancer*, 2005, **41**, 1203-1212.
62. C. Loo, A. Lin, L. Hirsch, M. H. Lee, J. Barton, N. Halas, J. West and R. Drezek, *Tech Cancer Res Tr*, 2004, **3**, 33-44.
63. D. P. O'Neal, L. R. Hirsch, N. J. Halas, J. D. Payne and J. L. West, *Cancer Lett*, 2004, **209**, 171-176.
64. X. J. Ji, R. P. Shao, A. M. Elliott, R. J. Stafford, E. Esparza-Coss, J. A. Bankson, G. Liang, Z. P. Luo, K. Park, J. T. Markert and C. Li, *J Phys Chem C*, 2007, **111**, 6245-6251.
65. S. E. Skrabalak, L. Au, X. M. Lu, X. D. Li and Y. N. Xia, *Nanomedicine*, 2007, **2**, 657-668.
66. M. P. Melancon, W. Lu, Z. Yang, R. Zhang, Z. Cheng, A. M. Elliott, J. Stafford, T. Olson, J. Z. Zhang and C. Li, *Mol Cancer Ther*, 2008, **7**, 1730-1739.
67. W. Lu, C. Xiong, G. Zhang, Q. Huang, R. Zhang, J. Z. Zhang and C. Li, *Clin Cancer Res*, 2009, **15**, 876-886.
68. J. Stern, J. Stanfield, W. Kabbani, J. Hsieh and J. Cadeddu, *J Urol*, 2008, **179**, 748-753.
69. R. Nadejda and Z. JinZhong, *Sci China Ser B-Chem*, 2009, **52**, 1559-1575.
70. H. M. Azzazy and M. M. Mansour, *Clin Chim Acta*, 2009, **403**, 1-8.
71. J. J. Diao and H. Chen, *J Chem Phys*, 2006, **124**.
72. B. Pelaz, V. Grazu, A. Ibarra, C. Magen, P. del Pino and J. M. de la Fuente, *Langmuir*, 2012, **28**, 8965-8970.
73. A. M. Schwartzberg, C. D. Grant, T. van Buuren and J. Z. Zhang, *J Phys Chem C*, 2007, **111**, 8892-8901.
74. G. Zhang, J. B. Jasinski, J. L. Howell, D. Patel, D. P. Stephens and A. M. Gobin, *Nanoscale Res Lett*, 2012, **7**, 337.
75. H. S. Zhou, I. Honma, H. Komiyama and J. W. Haus, *Phys Rev B*, 1994, **50**, 12052-12056.
76. T. J. Norman, J. Christian, D. Grant, D. Magana, J. Z. Zhang, J. Liu, D. Cao, F. Bridges and A. Van Buuren, *J Phys Chem B*, 2002, **106**, 7005-7012.
77. G. D. Zhang, X. H. Sun, J. Jasinski, D. Patel and A. M. Gobin, *J Nanomater*, 2012.
78. D. Patel, K. T. James, M. O'Toole, G. Zhang, R. S. Keynton and A. M. Gobin, *J Colloid Interf Sci*, 2015, **441**, 10-16.
79. W. S. Rasband, *ImageJ*, (1997-2011) National Institute of Health, Bethesda, MD.
80. *Minitab 16 Statistical Software 2010*, (2010), State College, PA.
81. O. Y. Uryupina, V. V. Vysotskii, V. V. Matveev, A. V. Gusef'nikova and V. I. Roldughin, *Colloid J*, 2011, **73**, 551-556.
82. J. E. Millstone, S. J. Hurst, G. S. Metraux, J. I. Cutler and C. A. Mirkin, *Small* 2009, **5**, 646-664.
83. J. K. Young, E. R. Figueroa and R. A. Drezek, *Ann Biomed Eng*, 2012, **40**, 438-459.
84. T. Kim, K. Lee, M.-s. Gong and S.-W. Joo, *Langmuir*, 2005, **21**, 9524-9528.
85. S. Gosh and T. Pal, *Chem Rev*, 2007, **107**, 4797-4862.
86. A. N. Shipway, M. Lahav, R. Gabai and I. Willner, *Langmuir*, 2000, **16**, 8789-8795.
87. Z. Guo, X. Fan, L. Xu, X. Lu, C. Gu, Z. Bian, N. Gu, J. Zhang and D. Yang, *Chem Commun (Camb)*, 2011, **47**, 4180-4182.
88. T. H. Ha, Y. J. Kim and S. H. Park, *Chem Commun (Camb)*, 2010, **46**, 3164-3166.